Empirical and Theoretical Calculations of *L*-subshell Coster-Kronig transitions in atoms with $28 \leq Z \leq 98$

Samia Meddah[1,2], Abdelhalim Kahoul[1,2*], Fernando Parente[3], Yazid Kasri[4,5], Jorge Miguel Sampaio[6,7], José Pires Marques[6,7], Stephen Croft[8], Andrea Favalli[9,10], Erhan Cengiz[11], Salim Daoudi[1,2]

[1]*Department of Matter Sciences, Faculty of Sciences and Technology, Mohamed El Bachir El Ibrahimi University, Bordj-Bou-Arreridj 34030, Algeria.*
[2]*Laboratory of Materials Physics, Radiation and Nanostructures (LPMRN), Faculty of Sciences and Technology, Mohamed El Bachir El Ibrahimi University, Bordj-Bou-Arreridj 34030, Algeria.*
[3]*Laboratory of Instrumentation, Biomedical Engineering and Radiation Physics (LIBPhys-UNL), Department of Physics, NOVA School of Science and Technology, NOVA University Lisbon, 2829-516 Caparica, Portugal.*
[4]*Physics Department, Faculty of Sciences, University of Mohamed Boudiaf, 28000 M'sila, Algeria.*
[5]*Theoretical Physics Laboratory, Faculty of Exact Sciences, University of Bejaia, 06000 Bejaia, Algeria.*
[6]*LIP – Laboratório de Instrumentação e Física Experimental de Partículas, Av. Prof. Gama Pinto 2, 1649-003 Lisboa, Portugal.*
[7]*Faculdade de Ciências da Universidade de Lisboa, Campo Grande, C8, 1749-016 Lisboa, Portugal.*
[8]*School of Engineering, Faculty of Science of Technology, Nuclear Science & Engineering Research Group, Lancaster University, Bailrigg, Lancaster, LA1 4YW, United Kingdom.*
[9]*European Commission, Joint Research Centre, Ispra, I-21027, Italy.*
[10]*Los Alamos National Laboratory, P.O. Box 1663, Los Alamos, NM 87545, USA.*
[11]*Department of Fundamental Sciences, Rafet Kayış Engineering Faculty, Alanya Alaaddin Keykubat University, 07425 Alanya/Antalya, Türkiye.*

*Corresponding author. Tel. /Fax (+213) 035862230.
E-mail address: *a.kahoul@univ-bba.dz*

Abstract: This work presents a comprehensive analytical investigation of Coster–Kronig transition probabilities f_{12}, f_{13}, f_{23}, F_1, and F_{123} for elements with atomic numbers $28 \leq Z \leq 98$. Experimental data from our previous studies were systematically compiled and employed to construct smooth empirical trends by polynomial interpolation so as to represent the variation of these transitions across the different elements. In parallel, new theoretical values were calculated for selected elements using the Multiconfiguration Dirac–Fock (MCDF) method, incorporating relativistic effects. When compared with available theoretical and experimental data the results show good agreement, especially for medium and heavy elements. These new results provide reliable reference data for modeling *L*-shell vacancy decay processes and support a range of applications in atomic physics, X-ray spectroscopy, and radiation interaction studies.

Keywords: X-ray fluorescence, Coster-Kronig transitions, empirical and MCDF calculations

1. Introduction

Accurate knowledge of atomic parameters is essential in various fields of physics and technology, including atomic spectroscopy, plasma physics, astrophysics, and materials science. Recent research highlights the growing importance of analytical techniques in this area, particularly around X-ray fluorescence, Coster–Kronig (CK) transitions, and Auger processes, as they are crucial for the quantitative analysis of materials and for determining parameters such as ionization and excitation cross-sections, based on observed spectra. Atomic parameters have been the subject of extensive theoretical and experimental investigations since the mid 20th century, leading to a substantial body of knowledge. This foundation continues to support the development of atomic models, enhancing our understanding of microphysical phenomena [1].

CK transitions are non-radiative processes in which a vacancy is transferred from one subshell to another within the same shell (e.g. L_2 to L_3), with the ejection of a higher-shell electron. These processes are highly sensitive to even minor variations in binding energy, particularly as the atom nears its energetic threshold. A slight shift in the element's energy can unlock a transition that was previously forbidden, leading to an abrupt change in its emission behaviour [2]. For instance, a vacancy can move from subshell L_1 to sub-shells L_2 or L_3 or, equivalently, an electron can move from sub-shells L_2 or L_3 to sub-shell L_1. The CK yield f_{ij}, where i and j denote the two subshells involved in the move, quantifies how likely this process is to happen. Explicitly, f_{12} is defined as the probability that a vacancy will move from L_1 to L_2, with an electron being ejected from a higher shell. Similarly, f_{13} is the probability of a vacancy moving from L_1 to L_3, and f_{23} is the probability

of a vacancy moving from L_2 to L_3. In addition, the combined coefficients can be expressed in a compact form as: $F_{123} = f_{12} \times f_{23} + f_{13}$ and $F_1 = f_{12} + f_{13}$ [3].

In the literature, investigations of L-subshell CK transitions have employed a variety of experimental approaches, contingent upon the specific ionization mechanism, the nature of the target material, and the characteristics of the detection systems, as well as diverse computational methodologies.

Important studies have been conducted previously on the measured and calculated L-subshell CK coefficients for several elements, often presented in tabular form. Fink et al. [4] reviewed the experimental data of the f_{ij} parameters that were published before 1966. Bambynek et al. [5] provided a compilation of experimental values for Coster–Kronig transitions from barium to curium. Krause [6] presented semi-empirical fitted values for L-subshell Coster–Kronig transitions, for elements with atomic numbers $22 \leq Z \leq 110$ using all experimental data available before 1979. Crasemann et al. [7] computed Coster–Kronig transition probabilities within a non-relativistic atomic model based on screened hydrogenic wave functions in the $j-j$ coupling framework, assuming a spherically symmetric potential. The same authors [2] computed L-subshell CK transition rates for 25 elements in the atomic range $70 \leq Z \leq 96$, in the framework of a relativistic Dirac-Hartree-Slater (DHS) model. They utilized perturbation theory with fixed orbitals and assessed both direct and exchange matrix elements, including relativistic two-electron interactions. The continuum wave functions were derived using the same atomic potential to maintain uniformity (self-consistency), and relaxed-orbital energies were employed for the extremely energy-sensitive CK transitions. Puri et al. [8] compiled f_{ij} $(ij = 12, 13, \text{and } 23)$ coefficients for all elements in the atomic number range $25 \leq Z \leq 96$, using radiative and non-

radiative transition rates obtained in the relativistic Dirac-Hartree-Slater (RDHS) model and used logarithmic interpolation of the original CK results of Chen and Crasemann. [2]. In 2015, Sampaio et al. [1] focused on the L-subshell CK transitions, obtaining improved relativistic values for several elements. Furthermore, Guerra et al. [9] published values of CK coefficients f_{ij} in nickel, obtained both theoretically and experimentally.

Concerning empirical methods, important work has been published on $f_{12}, f_{13},$ and f_{23} values for a wide range of elements. Öz et al. [10] used a least-squares approach with third-degree polynomial functions as a function of the atomic number to fit the experimentally obtained yields (f_{12}, f_{13}, f_{23}) in their work on C–K transitions and achieved high degree of agreement with the experimental data. These empirical functions reveal significant discontinuities, especially for f_{13}, in the region $Z = 75 - 80$, ascribed to changes in the character of electronic transitions, and they also provided useful tools for predicting values in situations when direct measurements are not possible.

In a recent paper [11], our research group presented empirical *L*-subshell CK transition probability values for the elements with the atomic number $50 \leq Z \leq 92$. In addition, we presented databases encompassing *L*-subshell CK transitions, including f_{12}, f_{13}, f_{23}, F_{123}, and F_1 yields. This extensive compilation includes experimental values published in 130 research papers spanning the years 1955 to 2024 for elements with atomic numbers $28 \leq Z \leq 100$.

We acknowledge that several compilations and theoretical evaluations of *L*-shell CK yields already exist in the literature [4-6]. Although several studies have focused on experimental and theoretical determination of *L*-shell CK yields, there is still a need for consistent and reliable empirical and semi-empirical data. Many previous experimental datasets suffer from limited energy resolution, restricted elemental coverage, or inconsistencies due to differences in excitation sources and detection systems. Likewise, theoretical models, while certainly useful, are often dependent on

specific approximations that may not fully reflect experimental realities. This creates a knowledge gap where empirical and semi-empirical approaches can offer a crucial synthesis of experimental measurements and theoretical trends until substantially new high quality experimental dataset are generated.

Our aim was not to duplicate these earlier works, but to provide a fully updated, unified, and simplified empirical framework that complements them and addresses current needs in both applications and future studies.

The novelty and contribution of our work can be summarized as follows:

- Integration of recent data and continuity with our first manuscript. Previously [3], we compiled and critically reviewed all available experimental results of *L*-shell CK yields spanning the last seven decades. This compilation, to our knowledge, was the first comprehensive and systematic collection of such data over this extended period. The present study builds directly upon that solid foundation: after assembling the complete dataset, we used it here to develop simplified empirical fits and comparisons, ensuring continuity between the two works. In addition, we have calculated the combined coefficients F_1, and F_{123}, which to our knowledge, had not been evaluated previously. These quantities are important because F_{123} is required to express the final vacancy distribution (V_3) in terms of the primary vacancy distribution (N_1, N_2, N_3) using the appropriate Coster–Kronig yields (f_{ij}). Moreover, F_{123} is also used to deduce key atomic parameters such as the average *L*-subshell fluorescence yields and the *L* X-ray production cross-sections. Similarly, F_1 represents the total L_1 CK probability, thereby providing an essential parameter for the accurate modeling of subshell de-excitation processes.

- New theoretical calculations: In addition to the empirical fits, we performed theoretical calculations using the MCDFGME code [25-26] for a set of elements. For some of these elements CK yields are calculated here for the first time. These new theoretical values expand the available database and provide additional benchmarks for comparison with both older compilations and our empirical results.
- Unified and practical fitting approach: Whereas earlier compilations often combined heterogeneous data without a common interpolation scheme, our approach applies a consistent polynomial fitting method across the entire dataset. This ensures a smooth and continuous representation that is easy to implement in practical contexts such as Monte Carlo simulations, XRF/PIXE studies, and radiation transport codes.

- Bridging gaps and highlighting weaknesses: In regions of Z where data remain sparse or uncertain, our fitted functions act as interpolative tools, offering approximate values while simultaneously highlighting where further experimental efforts are most urgently required. This is intended to provide both guidance and motivation for reinvigorated follow-up programs of study worldwide.
- Complementarity with theoretical models: Theoretical approaches (AHS, DHS, MCDF, etc.) provide first principles or physics-based insight. Our empirical framework does not replace these approaches ratherit serves as a complementary and practical resource, particularly where theoretical calculations are not yet available or remain computationally demanding.

As a continuation of our previous systematic work on the empirical calculation of fundamental atomic parameters such as fluorescence yields [12-22], the present study involves determining the

empirical values of CK transition yields f_{12}, f_{13}, f_{23}, F_{123}, and F_1 by using the experimental data provided in our previous work Meddah et al. [3], and new theoretical calculations for selected elements performed using the multiconfiguration Dirac-Fock (MCDF) method.

2. Calculation procedure of empirical Coster-Kronig transitions

The database of experimental values used in this work is the extensive compilation published recently by our group Meddah et al. [3]. In this investigation, we obtained empirical values of the L-shell CK coefficients f_{ij} $(ij = 12,13, \text{and } 23)$, F_{123}, and F_1, as a function of the atomic number Z, by direct interpolation of the experimental data, shown in Fig.1 (a, b, c, d, and e). For the first time, an empirical value of the f_{12} CK coefficient was determined using a dataset of 678 points. Similarly, the empirical f_{23} coefficient was calculated for the first time from 696 data points, while 585 points were used for the first computation of the empirical f_{13} CK coefficient. In addition, the experimental dataset for the F_{123} coefficient comprised 114 data points, and for the F_1 transition, 101 data points were employed.

To ensure reliable empirical CK coefficient values, we categorized the atomic data range for the f_{12} coefficient into two Z groups designatedthe low-Z region $40 \leq Z \leq 47$, and the medium- and high-Z region $50 \leq Z \leq 96$. Similarly, for f_{12}, we divided the atomic data range into two Z groups in this case $40 \leq Z \leq 90$ and $91 \leq Z \leq 96$. For f_{13}, F_{123} and F_1 the atomic data range was divided into three Z-groups, the low-Z region $39 \leq Z \leq 47$ for f_{13}, and $40 \leq Z \leq 47$ for F_{123} and F_1, the medium-Z region $50 \leq Z \leq 74$, and the high-Z region including $75 \leq Z \leq 98$ for f_{13}, and $75 \leq Z \leq 93$ for F_{123} and F_1. This choice was motivated by the observed trend of the CK transition values of Krause [6], Puri et al. [8], and McGuire [23]. Although this results in a discontinuous representation, the overall trend is captured reasonably well within the scatter of the experimental data, indicating that the

underlying structure is authentic. Our methodology therefore captures the essential features of the data while ensuring a reasonable and straightforward description across the entire atomic number range.

The polynomial functions used in the fitting process are:

$$\left(f_{ij}, F_1, F_{123}\right)_{\text{emp}} = \sum_{i=0}^{n} a_i Z^i = f(Z) \tag{1}$$

The fitted models are represented by solid lines in Figs. 1. The fitting coefficients a_i are summarized in Table 1. The overall deviation between the calculated empirical values of the f_{12}, f_{23}, f_{13}, F_{123}, and F_1 CK coefficients values and their corresponding experimental values is quantified using the root-mean-square error (ε_{RMS}), computed according to the following expression [12]:

$$\varepsilon_{\text{RMS}} = \left[\sum_{j=1}^{N} \frac{1}{N}\left(\frac{\chi_{j\text{expt}} - \chi_{j\text{calc}}}{\chi_{j\text{calc}}}\right)^2\right]^{\frac{1}{2}} \tag{2}$$

where N represents the total number of experimental data points, χ_{expt} denotes the experimental values, and χ_{calc} stands for the CK transition coefficients calculated using the polynomial fits to the respective data sets. The total root-mean-square error (ε_{RMS}) for the empirical results are provided in Table 1 for each coefficient.

Due to the absence of experimental data for elements $_{48}$Cd and $_{49}$In, the extrapolation method was used to estimate the empirical values of f_{23}, f_{13}, F_{123}, and F_1. In contrast, as the f_{12} value for element $_{49}$In was found to be negative, Puri's [24] data were employed to estimate the values for both elements $_{48}$Cd and $_{49}$In, by assuming a dependence of the form aZ^b using the relations [24]:

$$\mathrm{CK}(Z) = \mathrm{CK}(Z_2) \times (Z/Z_2)^b \qquad (3)$$

with $b = \frac{\log(\mathrm{CK}(Z_2)) - \log(\mathrm{CK}(Z_1))}{\log(Z_2) - \log(Z_1)}$; $\quad Z_1 \leq Z \leq Z_2$.

Z_1 and Z_2 denote the lower and higher atomic numbers, respectively, of elements for which CK transition emission rates are available on either side of the *Z*-interval where they are not available.

3. Relativistic calculations

L-shell vacancies are predominantly filled by radiationless transitions. Consequently, initial vacancy lifetimes are determined, in general, by Auger and CK transition rates. It has been found long ago that relativistic atomic models are needed for CK transition calculations. Non-relativistic models (such as the classical Hartree-Fock) showed a significant deviation from experimentally measured values, especially for elements with high atomic numbers [2].

In this work, f_{ij} (*ij*=12, 13, and 23), F_{123}, and F_1 CK coefficients are calculated using the relativistic computer code MCDFGME (version 2019), developed by Indelicato and Desclaux [25-26], that implements the multiconfiguration Dirac-Fock (MCDF) method. The code was used in the single-configuration approach, with the Breit interaction (both magnetic and retardation parts) and the leading-order vacuum polarization term (Uehling potential) included in the self-consistent field calculation. Other QED contributions, such as the electron self-energy and higher-order vacuum polarization terms, are included as perturbations. The wave functions and energies of the levels involved were optimized considering full relaxation of both initial and final states, to provide more accurate energies and wave functions. To deal with the nonorthogonality of the wavefunctions, the code uses the formalism described by Löwdin [9]. In treating the non-radiative transitions, we assumed a two-step process in which the decay is independent of the ionization, so that the electron ejected in the process of creation of the initial hole does not interact with the

emitted electron, and the core-hole state interacts very weakly with the latter electron, allowing for the transition rates to be calculated from perturbation theory. Continuum-state wave functions were obtained by solving the Dirac-Fock equations with the same atomic potential of the initial state, normalized to represent one ejected electron per unit energy. Multiconfiguration wave functions beyond intermediate coupling were not employed because the approximation used for the evaluation of the non-radiative rate cannot be used in an optimized level calculation with correlation orbitals [9]. For a more detailed description of the Hamiltonian and self-consistent field procedures, please refer to Indelicato et al. [27-29].

To facilitate the calculations, a special software package has been developed that can handle the level energies, transition rates, and partial sums needed to calculate the basic coefficients. In this package, all one- and two-gap configurations are automatically generated from the ground state configuration computed by the Dirac-Fock method, as described in Rodrigues et al. [30].

Assuming that the initial levels in the one-hole subshell S_n, with total angular momentum j_i, are statistically populated, the radiative (R) width of the subshell is obtained by summing the partial radiative widths Γ_{ij}^{R} over all initial levels i with one hole in the subshell, that decay radiatively to all final levels j in higher-energy subshells,

$$\Gamma_{S_n}^{\mathrm{R}} = \frac{\sum_{ij}(2j_i+1)\Gamma_{ij}^{\mathrm{R}}}{\sum_i(2j_i+1)}, \tag{4}$$

where the usual definition applies,

$$\Gamma_{ij}^{\mathrm{R}} = \hbar W_{ij}^{\mathrm{R}} . \tag{5}$$

Here W_{ij}^{R} is the radiative transition probability from level i to level j. Similarly, the non-radiative width of the subshell S_n is defined by:

$$\Gamma_{S_n}^{\mathrm{NR}} = \frac{\sum_{ik}(2j_i+1)\Gamma_{ik}^{\mathrm{NR}}}{\sum_i(2j_i+1)}, \tag{6}$$

where

$$\Gamma_{ik}^{\mathrm{NR}} = \hbar W_{ik}^{\mathrm{NR}} . \tag{7}$$

Here, W_{ik}^{NR} denotes the probability of a non-radiative transition from level i to level k. Thus, $\Gamma_{ik}^{\mathrm{NR}}$ represents the partial width associated with a non-radiative transition from an initial state i, containing a single vacancy in subshell S_n, to a final state k characterized by two vacancies located in the same shell or in higher energy shells or subshells. This process involves the emission of an electron into the continuum.

The CK $f_{S_{n,n'}}$ yield for the S_n subshell (S = L, M, or N) is given by a similar expression,

$$f_{S_{n,n'}} = \frac{\Gamma_{\mathrm{Sn}}^{\mathrm{NRCK}}}{\Gamma_{S_n}^{\mathrm{R}}+\Gamma_{S_n}^{\mathrm{NR}}} , \tag{8}$$

but, in this equation, only CK transitions are included in the $\Gamma_{S_n}^{\mathrm{NRCK}}$ width.

In Tables 2-6 The theoretical values are expressed to four significant figures for thirteen elements ($_{28}$Ni, $_{29}$Cu, $_{30}$Zn, $_{32}$Ge, $_{33}$As, $_{34}$Se, $_{36}$Kr, $_{48}$Cd, $_{50}$Sn, $_{52}$Te, $_{80}$Hg, $_{83}$Bi, $_{86}$Rn) for the CK coefficients f_{12}, f_{23}, f_{13}, F_{123}, and F_1 , respectively. These tables reveal an exceptional quantitative agreement between the empirical results and the theoretical calculations using the MCDF method. We performed empirical calculations for atomic numbers $40 \leq Z \leq 98$ due to the lack of available

empirical data. Notably, we found missing values in the range $30 \leq Z \leq 40$, which led us to choose the range from $_{40}$Zr and above for these calculations. In addition, we performed theoretical calculations covering the wider range $28 \leq Z \leq 98$. We did not use the values given in the reference [31] for tin (Z=50), because one of the values was markedly too high compared to the others

4. Results and discussion

In Tables 2, 3, 4, 5, and 6 we present, respectively, our calculated values of the empirical CK coefficients $(f_{12})_{\text{emp}}$, $(f_{23})_{\text{emp}}$, $(f_{13})_{\text{emp}}$, $(F_{123})_{\text{emp}}$, and $(F_1)_{\text{emp}}$ for all elements within the range $40 \leq Z \leq 98$, alongside the theoretical values, for elements $_{28}$Ni, $_{29}$Cu, $_{30}$Zn, $_{32}$Ge, $_{33}$As, $_{34}$Se, $_{36}$Kr, $_{48}$Cd, $_{50}$Sn, $_{52}$Te, $_{80}$Hg, $_{83}$Bi, and $_{86}$R.

To effectively compare our empirical and theoretical CK results with those from other authors, including experimental, theoretical, and fitted values, the present results are plotted in Fig. 2, as a function of the atomic number *Z*. We make the following observations:

For the empirical values of $(f_{12})_{\text{emp}}$ depicted in Fig. 2-(a) and calculated using Eq. (1), the comparison reveals satisfactory agreement between our results and those obtained experimentally [10,32,33], theoretically [2,7], and through fitting methods [6,8,23,34,35], across all elements ranging from $_{40}$Zr to $_{96}$Cm. The results of this study show excellent agreement with some experimental references, mainly Öz et al. [10], with low percentage differences $\text{RD}(\%) = \left|\left((f_{ij})_{\text{exp}} - (f_{ij})_{\text{emp}}\right)/(f_{ij})_{\text{emp}}\right| \times 100$ for some elements, such as 0% in ($_{86}$Rn) and 3.93% in ($_{57}$La) although we observe high differences for others such as ~33% in the case of ($_{84}$Po) and ~31% for ($_{93}$Np). Bansal et al. [33] data also show remarkable agreement, especially in heavy elements, where the percentage differences ranged from ~11% to ~19%. Except for $_{62}$Sm (~33%), the

differences between our results and those of Söğüt et al. [32] ranged from ~17% to ~41%. The values for elements in the range $40 \leq Z \leq 50$ differ significantly from our results, exceeding 50%. However, for some elements, the relative deviation was modest being in the range ~2% to ~9%. When comparing our values to Krause [6], we observe excellent agreement, especially for elements such as $_{82}$Pb (0.83%), $_{80}$Hg (0.78%), $_{84}$Po (0.90%), and $_{86}$Rn (0.99%). In contrast, some references showed moderate variability, amongst them Puri et al. [8], with differences ranging from 2.1% to 66%, and Chen and Crasemann [2], with relative variability ranging from 4.6% to 30%. A notable variation was observed for some elements, for example $_{40}$Zr, $_{45}$Rh, $_{83}$Bi, and $_{80}$Hg.

Good agreement with Öz et al. [10], who also employed a fitting technique to derive the values, ranging from 3.4% to 16% across several elements was noted.

Mcguire [23], Campbell [34], and Campbell [34] showed moderate differences in some elements, explained by the different theoretical models adopted.

The examination of Fig. 2-(b) simplified the process of comparing the values of Crasemann et al. [7], and the ones obtained through fitting methods [6,8,23,35] with our empirical values of the $(f_{13})_{\text{emp}}$ CK coefficient computed using formula (1) across elements from $_{39}$Y to $_{98}$Cf. The present calculations are in close agreement, up to 7.2%, with those reported by Kaur et al. [36]. Furthermore, our data are in close agreement, between 1.5% and 14%, with the measurements of Öz et al. [10]. In addition, theoretical values show an acceptable agreement, between 1.1% and 17%, with Chen and Crasemann [2], and between 0.38% and 16% with Crasemann et al. [7]. However, noticeable discrepancies are observed for some elements, especially $_{50}$Sn, with Crasemann et al. [7], and $_{39}$Y with Chen and Crasemann [2]. The present calculations closely match

those reported by Campbell [34], with RD% values in the range 0.0% to 11%. Our results show strong agreement with Campbell's [34] results, particularly in the region of high atomic number ($Z \geq 77$), where the relative differences vary from 0.0% to 8.5%, for instance, $_{83}$Bi (0%), $_{82}$Pb (0.66%), and $_{80}$Hg (4.7%). This reflects the accuracy of the model used to represent heavy elements. Compared to Puri's [8] results, the agreement appeared more diverse, especially in the intermediate atomic number region ($Z = 50 - 71$) with differences ranging from 1.5% to 20%, for example, $_{52}$Te (1.9%), $_{60}$Nd (16%), and $_{68}$Er (20%). These deviations are relatively high but still within the acceptable limits in this range taking into account the overall uncertainties. For the elements with $Z = 39 - 49$, the largest differences were found in the comparison with the Puri et al. [8] data, with deviations ranging from ~20% to ~51%. When comparing our results with the Krause [6] values, good agreement is observed in most cases, with relative differences ranging between 0% and 20% except for the element $_{75}$Re. On the other hand, the comparison of our results with McGuire [23] ones showed more variability. While some elements, such as $_{74}$W (0.60%) and $_{60}$Nd (5.9%), showed good agreement, others, such as $_{50}$Sn and $_{44}$Ru (32%) showed a large deviation.

Regarding the $(f_{23})_{\text{emp}}$ CK coefficient, Fig. 2-c illustrates the progression of our empirical findings as a function of the atomic number *Z*, computed using formula (1) across elements spanning from $_{40}$Zr to $_{96}$Cm. The comparison encompasses theoretical [2,37], fitted results [6, 8,10,23,34], alongside experimental data [10,38]. The results of our study showed good agreement with the theoretical values published by Chen and Crasemann [2], with relative differences ranging from 0.71% to 12% except for $_{40}$Zr, $_{92}$U, and $_{94}$Pu. In comparison with the theoretical data of Crasemann et al. [7], relative deviations generally ranged from 7.4% to 30%. However, this divergence gradually decreased from *Z* = 50 up, reaching low values in the lanthanide series $Z = (57 - 71)$, where differences are from 0.0% in Yb to 9.2% in La, with a near perfect match (0%)

in $_{69}$Tm and $_{74}$W. In contrast, the comparison with the Campbell [34] data revealed a deviation of 43% in $_{40}$Zr, which gradually decreased to 12% in Ce. Within the $Z = 51 - 91$, it remained between 0.0% to 10%. It should be noted, however, that some of the actinides reverted to high deviations, especially $_{92}$U (37%) and $_{93}$Np (49%). For McGuire [23], deviations range, generally, from 0.67% to 19%, but are above 20% for some elements. Our results agree with Öz's [10] results. The comparison of the results of Krause [6] with the current calculations showed that most of the relative differences are concentrated within a narrow low value range between 2.7% and 9.8%, but, deviations exceeding 20% were recorded in $_{40}$Zr (25%), $_{92}$U (25%), $_{93}$Np (28%), $_{94}$Pu (28%), and $_{95}$Am (20%). Finally, the experimental results obtained by Öz et al. [10] and Gupta et al. [38]) show good agreement with the current calculations. Most differences are centered between 0.90% and 5.3%, except for somewhat higher deviations in $_{81}$Tl (7.8%) and $_{83}$Bi (7.3%). Similarly, the data showed excellent agreement for $_{78}$Pt (0.0%) and $_{74}$W (2.9%), within the same reference range (0%-5%), while high deviations were reported for $_{82}$Pb (7.9%) and $_{92}$U (29%).

For the empirical values of $(F_{123})_{\text{em}}$ and $(F_1)_{\text{emp}}$ depicted in Figs. 2 (d), 2 (e), the comparison reveals agreement between our results and those obtained experimentally [10,36], theoretically [2,7], and through fitting methods [6, 8,10,23,34,35], across all elements ranging from $_{40}$Zr to $_{96}$Cm. In general the empirical $(F_{123})_{\text{emp}}$ results show agreement with the results of the comparison between current calculations and other references. McGuire [23] exhibits a deviation of more than 20% compared to a low one of about 1.4%; Krause's [6] data are characterized by deviations between 0.0% and 8.7%, with exceptions for some elements. Acceptable agreement is found with Chen and Crasemann's [2] values, most of the differences being between 5.0% and 17%, with essentially perfect agreement for Sn (0%), while high deviations are seen for $_{80}$Hg (30%) and $_{96}$Cm (25%). Some of Puri's [8] values exceeded a 30% deviation. Campbell's [34] data show deviations

between 0.60% and 14%. For Öz et al. [10], most of the differences are located between 0.48% and 10%, except for three high deviations of 16%, 41% and 75%. On the other hand, Kaur's [36] results showed good agreement, and most of the differences fell between 0.6% and 6.6%. There were some extreme values of 12.5% although overall there is a acceptable agreement.

For $(F_1)_{\text{emp}}$ there are variations in the magnitude of the deviations observed between the experimental and semi-empirical values reported in the data of this study and those presented in the works of Chen and Crasemann [2], Krause [6], and Campbell [34] across some elements. The RD% values vary from 0% to 13%, especially across the lanthanide series and heavy elements, within the atomic range $Z = 60$ to $Z = 96$. The data exhibited good agreement overall, with elements such as $_{60}$Nd, $_{62}$Sm, $_{63}$Eu, $_{66}$Dy, and $_{64}$Gd having acceptable deviations considering the quality of the available experimental data. These results confirm the reliability of previous work, especially that of Mergerigro [23] for intermediate atomic number elements. However, the values for $_{50}$Sn are notably extreme: 72% for Crasemann and Chen [2], and 87% for Puri et al. [8]. Heavy elements such as $_{75}$Re and $_{76}$Os also show high values of 34% and 35%, respectively, as reported in Puri [8]. In general, most of the deviations fall within the scientifically accepted range of approximately 0.2% to 15%.

Our theoretical calculation results, using a Multiconfiguration Dirac-Fock Method, for the *L*-subshells of selected elements within the range $28 \leq Z \leq 98$, are presented in Tables 2-6. Good agreement is observed between our results and those obtained experimentally [2,7,10,33], theoretically [2,7], and through fitting methods [6, 8,10,23,34,35], across all elements with atomic numbers ranging from $_{28}$Ni to $_{96}$Cm.

In Fig. 2, we can see that our newly calculated theoretical values are generally in good agreement with other works. However, discrepancies exist for specific elements when compared with the

theoretical values of Puri et al. [8], showing an RD% range from 0% to 12%. A ~9% deviation is observed for element $_{36}$Kr. Similarly, comparing our theoretical results with the calculations of Cresmann and Chen [2], we find RD% values ranging from 4% to 8%, with significant deviations for elements $_{33}$As, $_{50}$Sn, $_{53}$I, and $_{56}$Ba. The fitted results of Campell [34,35] generally show a good agreement, in the range of 1.5% to 25%. The results of Krause [6] also exhibit good agreement. However, higher deviations occur for elements $_{80}$Hg, $_{83}$Bi, $_{86}$Rn observed for Puri et al. [8], and the fitted calculations by Öz et al. [10] also reveal disagreements across certain atomic number ranges. While our theoretical calculations typically exhibit strong agreement with empirical values, there are noteworthy disparities for specific elements within the range $28 \leq Z \leq 40$ when compared to the theoretical values of Krause [6], the fitted calculations of Puri et al. [8], and Campbell [34].

Regarding the f_{23} CK coefficients, discrepancies emerge for $Z < 40$, when comparing empirical results to specific theoretical and fitted values, as, for instance, relative to the theoretical values of Crasemann and Chen [2]. However, in the same Z range, there exists general alignment with Puri et al. [8] and Krause [6] values. On the other hand, for Z values exceeding 40, generally we find good agreement, at the 1.3% level, with previous values. Furthermore, consensus is found with the values of Campbell [34], Puri et al. [8] Öz et al. [10], and Mcguire [23]. Regarding the currently calculated theoretical values, they largely concur, yet variations surface notably for $_{50}$Sn and $_{51}$Sb.

Our present theoretical values are graphically compared with other values for the f_{13}, F_1 , F_{123} in Fig. 2. Upon analysis of Fig. 2 (c), (d), and (e). Within the range of $28 \leq Z \leq 40$, disparities emerge between the results of our theoretical calculations and the theoretical or fitted values from other researchers, including the theoretical values of Krause [6], the fitted values of Puri et al. [8], and the experimental data from Campbell [34] and Kaur et al. [36]. On the other hand, our

theoretical calculations demonstrate good agreement with other works. For instance, the fitted results of Krause [6] and McGuire [23] exhibit good agreement within the range of $40 \leq Z \leq 98$.

Our present theoretical values are graphically compared with our empirical results for the f_{12}, f_{23}, f_{13}, F_{123}, and F_1 in Fig. 2. It can be seen that within the range of $40 \leq Z \leq 98$, the empirical and theoretical CK coefficients exhibit a very good alignment with those from our empirical groups across the entire atomic number.

A comprehensive comparative analysis between the results of this study and both theoretical and experimental literature demonstrates broad agreement in the representation of calculated values. This concordance across atomic number and transition parameter reinforces the credibility of the models employed and validates the accuracy of the applied methods. Nevertheless, the observed scatter indicates significant potential for improvement through the acquisition of new, high-quality experimental measurements. Such enhancements would enable tighter constraints on empirical and semi-empirical representations and provide a more rigorous benchmark for first-principles theoretical calculations.

Conclusion

This study focused on calculating empirical Coster–Kronig (CK) transition coefficients – f_{12}, f_{23}, f_{13}, F_{123}, and F_1– using an interpolation approach applied to experimental data extracted from an extensive modern database. In parallel, first-principles theoretical calculations were performed using the Multiconfiguration Dirac–Fock method for eight representative elements. The results exhibit relatively good agreement with those reported by other research groups, underscoring the importance of integrating empirical and theoretical approaches to coherently characterize the spectroscopic properties of materials across a wide dynamic range. The interpolation-based method

for empirical CK transitions yielded ostensively reliable values that can be readily incorporated into formulas and computational codes for determining X-ray ionization and production cross-sections. However, the study also identified cases where deviations exceeded the expected accuracy of both experimental and theoretical predictions, highlighting the need for further high-quality investigations. In this context, acquiring more precise and accurate experimental data – particularly for specific atomic numbers where current measurements are lacking – is essential. Incorporating these benchmarks will enhance the reliability and applicability of the findings, thereby advancing our understanding of spectroscopic properties throughout the periodic table.

5. Acknowledgments

We gratefully acknowledge the support of the DGRSDT, Ministry of Higher Education and Scientific Research, Algeria. This work was done with the support of Mohamed El Bachir El Ibrahimi University, under project (PRFU) No: B00L02UN340120230001. This work was also supported by the Fundação para a Ciência e Tecnologia (FCT), Portugal through contracts UIDP/50007/2020 (LIP) and UID/FIS/04559/2020 (LIBPhys). S.C. warmly acknowledges the support of Lancaster University, and A.F. gratefully acknowledges the support of the Joint Research Centre of the European Commission.

Figure captions:

Fig. 1. Distribution of the experimental (a): $(f_{12})_{\mathrm{exp}}$, (b): $(f_{23})_{\mathrm{exp}}$, (c): $(f_{13})_{\mathrm{exp}}$, (d): $(F_{123})_{\mathrm{exp}}$, and (e): $(F_1)_{\mathrm{exp}}$ values as a function of the atomic number *Z*. The curve is the interpolation, according to Eq. (1).

Fig. 2. The empirical values of the Coster-Kronig coefficients and the theoretical values (MCDFGME), (a): $(f_{12})_{\mathrm{emp}}$, (b): $(f_{23})_{\mathrm{emp}}$, (c): $(f_{13})_{\mathrm{emp}}$, (d): $(F_{123})_{\mathrm{emp}}$, and (e): $(F_1)_{\mathrm{emp}}$, compared to the empirical, semi-empirical, theoretical and experimental values of other authors.

References

[1] J.M. Sampaio, T.I. Madeira, M. Guerra, F. Parente, J.P. Santos, P. Indelicato, J.P. Marques, Dirac–Fock calculation of K-, L-, and M-shell fluorescence and Coster–Kronig yields for Ne, Ar, Kr, Xe, Rn, and Uuo, *Phys. Rev. A* 91 (2015) 052507, https://doi.org/10.1103/PhysRevA.91.052507.

[2] M.H. Chen, B. Crasemann, and H. Mark, Widths and fluorescence yields of atomic L-shell vacancy states, *Phys. Rev. A*, vol. 24, no. 1, pp. 177–182, Jul. 1981, doi:10.1103/PhysRevA.24.177.

[3] S. Meddah, A. Kahoul, F. Parente, S. Daoudi, J.P. Marques, J.M. Sampaio, S. Croft,

A. Favalli, Y. Kasri, N.K. Kup Aylikci, V. Aylikci, A. Hamidani, L-subshell experimental Coster–Kronig probabilities and Auger decays for elements in the atomic number range $28 \leq Z \leq 100$, *Atomic Data and Nuclear Data Tables* 164 **(**2025**)** 101731, https://doi.org/10.1016/j.adt.2025.101731.

[4] R.W. Fink, R.C. Jopson, H. Mark, C.D. Swift, Atomic fluorescence yields, *Rev. Mod. Phys.* 38 (1966) 513–540, https://doi.org/10.1103/RevModPhys.38.513.

[5] W. Bambynek, B. Crasemann, R.W. Fink, H.-U. Freund, H. Mark, C.D. Swift, R.E. Price, P.V. Rao, X-Ray fluorescence yields, Auger, and Coster–Kronig transition probabilities, *Rev. Mod. Phys.* 44 (1972) 716–813, https://doi.org/10.1103/RevModPhys.44.716.

[6] M.O. Krause, Atomic radiative and radiationless yields for K and L shells, *J. Phys. Chem. Ref. Data* 8 (1979) 307–327, https://doi.org/10.1063/1.555594.

[7] B. Crasemann, M.H. Chen, V.O. Kostroun, Auger and Coster–Kronig transition probabilities to the atomic 2s state and theoretical L_1 fluorescence yields, *Phys. Rev. A* 4 (1971) 2161–2164, https://doi.org/10.1103/PhysRevA.4.2161.

[8] S. Puri, D. Mehta, B. Chand, N. Singh, P.N. Trehan, *L-shell fluorescence yields and Coster–Kronig transition probabilities for elements with* $25 \leq Z \leq 96$, *X-Ray Spectrom.* 22 (1993) 358–361, https://doi.org/10.1002/xrs.1300220507.

[9] M. Guerra, J.M. Sampaio, F. Parente, P. Indelicato, P. Hönicke, M. Müller, B. Beckhoff, J.P. Marques, J.P. Santos, Theoretical and experimental determination of K- and L-shell x-ray relaxation parameters in Ni, *Phys. Rev. A* 97 **(**2018**)** 042501, https://doi.org/10.1103/PhysRevA.97.042501.

[10] E. Öz, N. Ekinci, Y. Özdemir, M. Ertuğrul, Y. Şahin, H. Erdogan, Measurement of atomic L-shell Coster—Kronig yields (f_{12}, f_{23} and f_{13}) for some elements in the atomic number range $59 \leq Z \leq 90$, J. Phys. B: At. Mol. Opt. Phys. 34 (2001) 631–638, https://doi.org/10.1088/0953-4075/34/4/311.

[11] V. Aylikçi, A. Kahoul, N.K. Kup Aylikçi, E. Tiraşoğlu, İ.H. Karahan, A. Abassi, M. Dogan, Empirical and semi-empirical interpolation of L X-ray fluorescence parameters for elements in the atomic range $50 \leq Z \leq 92$, *Radiat. Phys. Chem.* 106 (2015) 99–125, https://doi.org/10.1016/j.radphyschem.2014.06.030.

[12] A. Kahoul, A. Abassi, B. Deghfel, M. Nekkab, K-shell fluorescence yields for elements with $6 \leq Z \leq 99$, *Radiat. Phys. Chem.* 80 **(**2011**)** 369–377,

https://doi.org/10.1016/j.radphyschem.2010.11.011.

[13] N. Küp Aylikçi, V. Aylikçi, A. Kahoul, E. Tirasoglu, I.H. Karahan, E. Cengiz, Effect of pH treatment on K x-ray intensity ratios and K x-ray production cross sections in ZnCo alloys, *Phys. Rev. A* 84 (2011), 042509, https://doi.org/10.1103/PhysRevA.84.042509.

[14] S. Daoudi, A. Kahoul, Y. Sahnoune, B. Deghfel, Y. Kasri, F. Khalfallah, M. Nekkab, New K-shell fluorescence yields curve for elements with $3 \leq Z \leq 99$, *J. Korean Phys. Soc.* 67 (2015), 1537–1543, https://doi.org/10.3938/jkps.67.1537.

[15] A. Bendjedi, B. Deghfel, A. Kahoul, I. Derradj, F. Khalfallah, Y. Sahnoune, A. Bentabet, M. Nekkab, L-shell fluorescence yields and total ionization and X-ray production cross sections for elements with $40 \leq Z \leq 92$, *Radiat. Phys. Chem.* 117 (2015) 128–134, https://doi.org/10.1016/j.radphyschem.2015.08.008.

[16] Y. Sahnoune, A. Kahoul, Y. Kasri, B. Deghfel, D. E. Medjadi, F. Khalfallah, S. Daoudi, V. Aylikçi, N. Küp Aylikçi, M. Nekkab, L_1, L_2, and L_3 subshell fluorescence yields: Updated database and new empirical values, *Radiat. Phys. Chem.* 125 (2016) 227–251, https://doi.org/10.1016/j.radphyschem.2016.04.016.

[17] Y. Sahnoune, A. Kahoul, S. Daoudi, J.M. Sampaio, N.K. Aylikçi, V. Aylikçi, Y. Kasri, B. Deghfel, J.P. Marques, D.E. Medjadi, Updated database, new empirical and theoretical values of average L shell fluorescence yields of elements with $23 \leq Z \leq 96$, *Radiat. Phys. Chem.* 166 (2020) 108495, https://doi.org/10.1016/j.radphyschem.2019.108495.

[18] A. Hamidani, S. Daoudi, A. Kahoul, J.M. Sampaio, J.P. Marques, F. Parente, S. Croft, A. Favalli, N.K. Kup Aylikci, V. Aylikci, Y. Kasri, K. Meddouh, Updated database, semi-empirical and theoretical calculation of Kβ/Kα intensity ratios for elements ranging from $_{11}$Na to $_{96}$Cm, *Atomic Data and Nuclear Data Tables* 149 (2023) 101549, https://doi.org/10.1016/j.adt.2022.101549.

[19] B. Berkani, A. Kahoul, J.M. Sampaio, S. Daoudi, J.P. Marques, F. Parente, A. Hamidani, S. Croft, A. Favalli, Y. Kasri, A. Zidi, K. Amari, Vacancy transfer probability parameters: Database and a new empirical value for elements in the atomic number range $16 \leq Z \leq 92$, *Radiat. Phys. Chem.* 225 (2024) 112106, https://doi.org/10.1016/j.radphyschem.2024.112106.

[20] K. Amari, A. Kahoul, J.M. Sampaio, Y. Kasri, J.P. Marques, F. Parente, A. Hamidani, S. Croft, A. Favalli, S. Daoudi, B. Deghfel, A. Zidi, B. Berkani, Empirical calculation of K-shell fluorescence cross sections for elements in the atomic range $16 \leq Z \leq 92$ by photon effects ranging from 5.46 to 123.6 keV (Three-dimensional formulae), *Phys. Scr.* 99 (2024) 105402, https://doi.org/10.1088/1402-4896/ad720e.

[21] B. Berkani, A. Kahoul, J.M. Sampaio, S. Daoudi, J.P. Marques, F. Parente, A. Hamidani, S. Croft, A. Favalli, Y. Kasri, A. Zidi, K. Amari, Relativistic and semi-theoretical calculations of K-shell to L-shell/subshell vacancy transfer probabilities, *Spectrochimica Acta Part B: Atomic Spectroscopy* 224 (2025) 107089, https://doi.org/10.1016/j.sab.2024.107089.

[22] A. Zidi, S. Kahoul, J.M. Marques, A. Daoudi, J.P. Sampaio, F. Parente, A. Hamidani, S. Croft, A. Favalli, Y. Kasri, B. Berkani, K. Amari, *Theoretical, empirical, and semi-empirical insights into L-shell X-ray intensity ratios*, *At. Data Nucl. Data Tables* 152 (2025) 101645, https://doi.org/10.1016/j.adt.2024.101645.

[23] E.J. McGuire, Atomic L-shell Coster-Kronig, Auger, and radiative transitions for $12 \leq Z \leq 106$, *Phys. Rev. A* **3** (1971), 587–604, https://doi.org/10.1103/PhysRevA.3.587.

[24] S. Puri, Relative intensities for Li (i = 1–3) and Mi (i = 1–5) subshell X-rays, *At. Data Nucl. Data Tables* 93 (2007) 730–741, https://doi.org/10.1016/j.adt.2007.05.002.

[25] J.P. Desclaux, A multiconfiguration relativistic Dirac–Fock program, *Comput. Phys. Commun.* 9 (1975) 31–45, https://doi.org/10.1016/0010-4655(75)90054-5.

[26] P. Indelicato, J.P. Desclaux, MCDFGME: A multiconfiguration Dirac–Fock and general matrix elements program, *arXiv:physics/0701239* (2007), https://doi.org/10.48550/arXiv.physics/0701239.

[27] P. Indelicato, O. Gorceix, J.P. Desclaux, Multiconfigurational Dirac–Fock studies of two-electron ions. II. Radiative corrections and comparison with experiment, *J. Phys. B: At. Mol. Opt. Phys.* 20 (1987) 651–663, https://doi.org/10.1088/0022-3700/20/4/007.

[28] P. Indelicato, J.P. Desclaux, Multiconfiguration Dirac–Fock calculations of transition energies with QED corrections in three-electron ions, *Phys. Rev. A* 42 (1990) 5139–5149, https://doi.org/10.1103/PhysRevA.42.5139.

[29] P. Indelicato, Correlation and negative continuum effects for the relativistic M1 transition in two-electron ions using the Multiconfiguration Dirac–Fock method, *Phys. Rev. Lett.* 77 (1996) 3323–3326, https://doi.org/10.1103/PhysRevLett.77.3323.

[30] G.C. Rodrigues, P. Indelicato, J.P. Santos, P. Patté, F. Parente, Systematic calculation of total atomic energies of ground state configurations, *At. Data Nucl. Data Tables* **86** (**2004**) 117–233, https://doi.org/10.1016/j.adt.2003.11.005.

[31] G. Ménesguen, P. Cugier, F. Dumas, J.F. Guillaud, G. Lacroix, A. Lefebvre, B. Liorzou, B. Thouvenin, Evaluation of the coastal eutrophication potential of French Atlantic estuaries and lagoons, *Cont. Shelf Res.* 141 (2017), 63–76 , https://doi.org/10.1016/j.csr.2017.04.008.

[32] Ö. Sögüt, Measurement of atomic L-subshell Coster-Kronig transition (f_{12}) for some elements in the atomic range $52 \leq Z \leq 92$, *Instrum. Sci. Technol.* 31 (2003) 85–92, https://doi.org/10.1081/CI-120018410.

[33] H. Bansal, M.K. Tiwari, R. Mittal, L subshell fluorescence cross-section measurements for elements $Z = 62$–67 at tuned photon energies, *J. Quant. Spectrosc. Radiat. Transf.* 199 (2017) 93–102, https://doi.org/10.1016/j.jqsrt.2017.05.007.

[34] J.L. Campbell, Fluorescence yields and Coster–Kronig probabilities for the atomic L subshells, *Atomic Data and Nuclear Data Tables* 85 (2003) 291–315, https://doi.org/10.1016/S0092-640X(03)00059-7.

[35] J.L. Campbell, Fluorescence yields and Coster–Kronig probabilities for the atomic L subshells. Part II: The L_1 subshell revisited, *Atomic Data and Nuclear Data Tables* **95** (**2009**) 115–124, https://doi.org/10.1016/j.adt.2008.08.002.

[36] G. Kaur, H. Bansal, M.K. Tiwari, R. Mittal, L subshell fluorescent X-ray measurements to study Coster–Kronig transitions in the $66 \leq Z \leq 83$ region, *Pramana – J. Phys.* 87 (2016) 33, https://doi.org/10.1007/s12043-016-1223-9.

[37] M.H. Chen, B. Crasemann, V.O. Kostroun, Auger and Coster–Kronig transition probabilities to the atomic 2s state and theoretical L_1 fluorescence yields, *Phys. Rev. A* 4 (1971), 2161–2164, https://doi.org/10.1103/PhysRevA.4.2161.

[38] N. Gupta, D. Mehta, S. Puri, B. Chand, N. Singh, P.N. Trehan, Radiative and radiationless transition probabilities for L subshells of elements with $40 \leq Z \leq 100$, *Radiat. Phys. Chem.* 79 (2010), 23–34, https://doi.org/10.1016/j.radphyschem.2009.07.010.

[39] P.-O. Löwdin, Quantum theory of many-particle systems. I. Physical interpretations by means of density matrices, natural spin-orbitals, and convergence problems in the method of configurational interaction, Phys. Rev. 97 (1955) 1474–1489, https://doi.org/10.1103/PhysRev.97.1474.

Fig. 1:

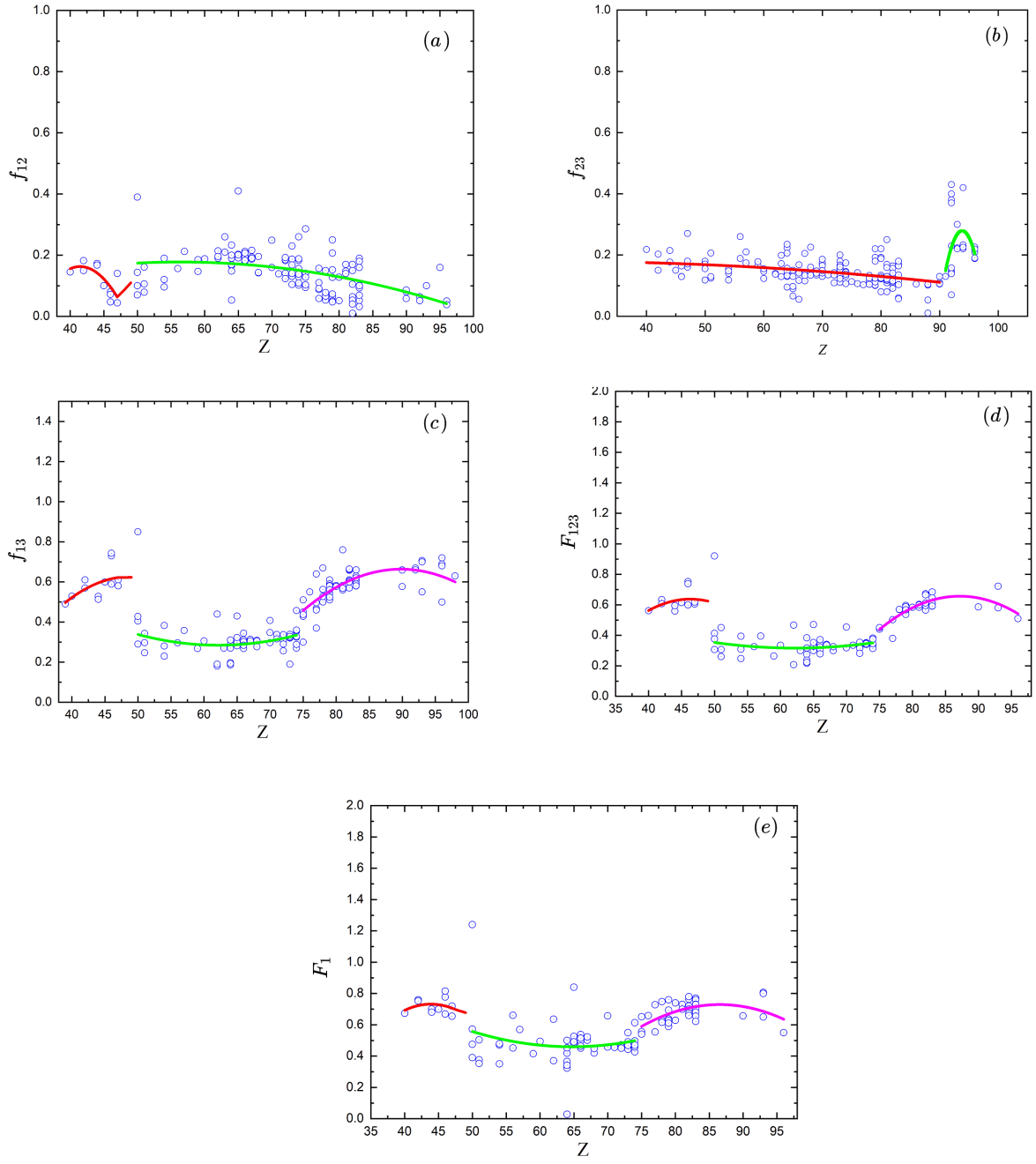

Fig. 2:

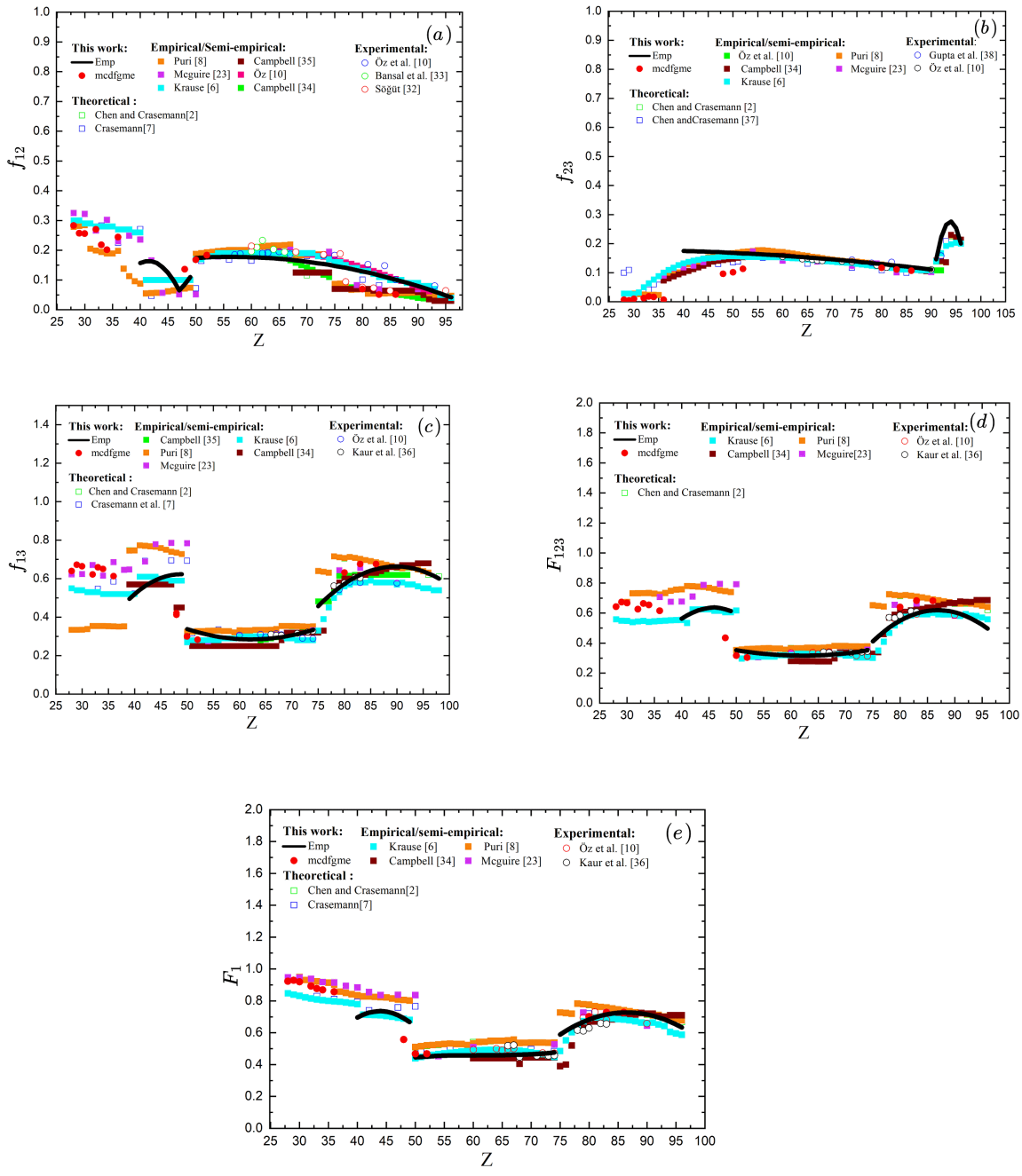

Table 1. Fitting coefficients according to Eq. (1).

Coster-Kronig Transitions	Z **-group**	**Parameters**	**Values**
f_{12}	$40 \leq Z \leq 47$	a_0	-5.44500
		a_1	0.27045
		a_2	-0.00326
		ε_{RMS}(%)=52.26	
	$50 \leq Z \leq 96$	a_0	-0.09553
		a_1	0.00971
		a_2	-0.00009
		ε_{RMS}(%)=34.22	
f_{13}	$39 \leq Z \leq 47$	a_0	-2.54706
		a_1	0.12987
		a_2	-0.00133
		ε_{RMS}(%)=9.59	
	$50 \leq Z \leq 74$	a_0	1.67473
		a_1	-0.04470
		a_2	0.00036
		ε_{RMS}(%)=26.6	
	$75 \leq Z \leq 98$	a_0	-6.94263
		a_1	0.16941
		a_2	-0.00094
		ε_{RMS}(%)=10.62	
f_{23}	$40 \leq Z \leq 90$	a_0	0.17068
		a_1	0.00072
		a_2	-0.00002
		ε_{RMS}(%)=9.1	
	$91 \leq Z \leq 96$	a_0	-142.459
		a_1	3.04220
		a_2	-0.01621
		ε_{RMS}(%)=39.38	
F_{123}	$40 \leq Z \leq 47$	a_0	-3.39811
		a_1	0.17423
		a_2	0.00188
		ε_{RMS}(%)=7.96	
	$50 \leq Z \leq 74$	a_0	1.27378
		a_1	0.03079
		a_2	0.00025
		ε_{RMS}(%)=27.99	
	$75 \leq Z \leq 93$	a_0	-10.5506
		a_1	0.25715

		a_2	-0.00148
		ε_{RMS}(%)=9.72	
F_1	$40 \leq Z \leq 47$	a_0	-4.33281
		a_1	0.23091
		a_2	-0.00263
		ε_{RMS}(%)=6.5	
	$50 \leq Z \leq 74$	a_0	-1.39738
		a_1	0.09042
		a_2	-0.00147
		a_3	0.00001
		ε_{RMS}(%)=30.3	
	$75 \leq Z \leq 98$	a_0	-7.13214
		a_1	0.18169
		a_2	-0.00105
		ε_{RMS}(%)=9.05	

Table 2: Empirical (this work), theoretical calculations, using the multiconfiguration Dirac-Fock method (MCDFGME), theoretical, empirical, semi-empirical, and experimental (other works) of the Coster Kroning transition probability f_{12} from $_{28}$Ni to $_{96}$Cm.

Z, element	This work		Other works								
			Theo.		Empirical/semi-empirical						
	Emp	MCDFGME	Chen and Crasemann [2]	Crasemann et al. [7]	Campbell [35]	Puri [8]	Campbell [34]	McGuire [23]	Öz et al. [10]	Krause [6]	Exp [k]Öz et al. [10] [m]Bansal et al. [33] [s]Söğüt [32]
$_{28}$Ni	-	0.283	-	-	-	0.279	-	0.325	-	0.30	-
$_{29}$Cu	-	0.257	-	-	-	0.282	-	-	-	0.30	-
$_{30}$Zn	-	0.256	0.284	-	-	0.284	-	0.322	-	0.29	-
$_{31}$Ga	-	-	-	-	-	0.205	-	-	-	0.29	-
$_{32}$Ge	-	0.270	-	-	-	0.199	-	0.266	-	0.28	-
$_{33}$As	-	0.218	-	0.282	-	0.194	-	-	-	0.28	-
$_{34}$Se	-	0.219	-	-	-	0.189	-	0.302	-	0.28	-
$_{35}$Br	-	-	0.190	-	-	0.189	-	-	-	0.28	-
$_{36}$Kr	-	0.244	0.198	0.225	-	0.198	-	-	-	0.27	-
$_{37}$Rb	-	-	-	-	-	0.138	-	0.230	-	0.27	-
$_{38}$Sr	-	-	-	-	-	0.113	-	0.249	-	0.27	-
$_{39}$Y	-	-	-	-	-	0.096	-	-	-	0.26	-
$_{40}$Zr	0.157	-	0.088	0.271	-	0.088	-	0.236	-	0.26	-
$_{41}$Nb	0.163	-	-	-	-	0.055	-	-	-	0.10	-
$_{42}$Mo	0.163	-	-	0.047	-	0.056	-	0.166	-	0.10	-
$_{43}$Tc	0.157	-	-	-	-	0.057	-	-	-	0.10	-
$_{44}$Ru	0.143	-	-	-	-	0.057	-	0.057	-	0.10	-
$_{45}$Rh	0.124	-	0.062	-	-	0.062	-	-	-	0.10	-
$_{46}$Pd	0.098	-	-	-	-	0.065	-	-	-	0.10	-
$_{47}$Ag	0.065	-	0.068	0.063	-	0.068	-	0.052	-	0.10	-
$_{48}$Cd	0.085	0.136	-	-	-	0.071	-	-	-	0.10	-
$_{49}$In	0.110	-	-	-	-	0.074	-	-	-	0.10	-
$_{50}$Sn	0.174	0.168	0.188	0.072	-	0.188	-	0.052	-	0.17	-
$_{51}$Sb	0.175	-	-	0.164	-	0.190	-	-	-	0.17	-
$_{52}$Te	0.176	0.184	0.192	-	-	0.193	-	-	-	0.18	-
$_{53}$I	0.177	-	-	-	-	0.195	-	-	-	0.18	-
$_{54}$X	0.177	-	0.196	-	-	0.197	-	0.179	-	0.19	-
$_{55}$Cs	0.178	-	-	-	-	0.199	-	-	-	0.19	-
$_{56}$Ba	0.178	-	0.200	0.168	-	0.201	-	-	-	0.19	-
$_{57}$La	0.178	-	-	-	-	0.201	-	-	-	0.19	-
$_{58}$Ce	0.177	-	-	-	-	0.201	-	-	-	0.19	-
$_{59}$Pr	0.177	-	-	-	-	0.201	-	-	0.183	0.19	0.185[k]
$_{60}$Nd	0.176	-	0.209	0.165	-	0.210	0.190	0.207	0.186	0.19	0.188[k]
$_{61}$Pm	0.176	-	-	-	-	0.211	0.190	-	0.189	0.19	-
$_{62}$Sm	0.175	-	-	-	-	0.212	0.190	-	0.191	0.19	0.196[m], 0.214[s]
$_{63}$Eu	0.174	-	0.214	-	-	0.215	0.190	-	0.193	0.19	0.21[m]
$_{64}$Gd	0.173	-	-	-	0.190	0.216	0.190	-	0.194	0.19	0.190[k], 0.233[m]
$_{65}$Tb	0.171	-	-	-	0.182	0.216	0.190	-	0.194	0.19	0.191[k], 0.203[m]
$_{66}$Dy	0.170	-	-	-	0.174	0.217	0.190	-	0.194	0.19	0.195[k], 0.194[m]
$_{67}$Ho	0.168	-	0.218	0.178	0.166	0.219	0.190	0.202	0.193	0.19	0.187[k], 0.19[m], 0.194[s]
$_{68}$Er	0.166	-	-	-	0.158	0.182	0.125	-	0.192	0.19	-

$_{69}$Tm	0.164	-	-	-	0.150	0.183	0.125	-	0.190	0.19	-
$_{70}$Yb	0.161	-	0.116	0.180	0.142	0.184	0.125	-	0.187	0.19	-
$_{71}$Lu	0.159	-	-	-	0.134	0.185	0.125	-	0.185	0.19	-
$_{72}$Hf	0.156	-	-	-	0.126	0.186	0.125	-	0.181	0.18	0.182^{k}, 0.185^{s}
$_{73}$Ta	0.154	-	-	-	0.118	0.186	0.125	-	0.178	0.18	
$_{74}$W	0.151	-	0.185	0.160	0.110	0.186	0.125	0.195	0.174	0.17	0.183^{k}, 0.188^{s}
$_{75}$Re	0.147	-	-	-	-	0.087	0.070	-	0.169	0.16	0.094^{s}
$_{76}$Os	0.144	-	-	-	-	0.088	0.070	-	0.164	0.16	-
$_{77}$Ir	0.141	-	-	-	0.076	0.088	0.070	-	0.159	0.15	-
$_{78}$Pt	0.137	-	-	-	0.075	0.067	0.070	-	0.154	0.14	0.076^{s}
$_{79}$Au	0.133	-	-	-	0.074	0.068	0.070	0.083	0.148	0.14	0.152^{k}, 0.073^{s}
$_{80}$Hg	0.129	0.069	0.069	0.101	0.072	0.069	0.070	-	0.142	0.13	-
$_{81}$Tl	0.125	-	-	-	0.069	0.054	0.070	-	0.136	0.13	0.148^{k}
$_{82}$Pb	0.121		-	-	0.066	0.054	0.064	-	0.130	0.12	0.064^{s}
$_{83}$Bi	0.116	0.051	0.0549	-	0.063	0.055	0.064	0.069	0.124	0.11	0.101^{k}
$_{84}$Po	0.111	-	-	-	0.060	0.055	0.064	-	0.117	0.11	-
$_{85}$At	0.106	-	-	0.082	0.057	0.056	0.064	-	0.110	0.10	-
$_{86}$Rn	0.101	0.051	-	-	0.053	0.056	0.064	-	0.103	0.10	-
$_{87}$Fr	0.096	-	-	-	0.050	0.056	0.064	-	0.097	0.10	-
$_{88}$Ra	0.091	-	-	-	0.047	0.056	0.064	-	0.090	0.09	-
$_{89}$Ac	0.085	-	-	-	0.044	0.057	0.064	-	0.083	0.09	-
$_{90}$Th	0.080	-	0.0575	-	0.040	0.058	0.060	0.069	0.076	0.09	0.080^{k}
$_{91}$Pa	0.074	-	-	-	0.038	0.053	0.050	-	0.069	0.08	-
$_{92}$U	0.068	-	0.051	-	0.035	0.051	0.035	-	0.062	0.08	0.064^{s}
$_{93}$Np	0.061	-	-	-	-	0.046	0.030	-	-	0.07	-
$_{94}$Pu	0.055	-	-	-	-	0.046	0.030	-	-	0.05	-
$_{95}$Am	0.048	-	-	-	-	0.047	0.030	-	-	0.05	-
$_{96}$Cm	0.042	-	0.047	-	-	0.047	0.030	-	-	0.04	-

Table 3: Empirical (this work), theoretical calculations, using the multiconfiguration Dirac-Fock method (MCDFGME), theoretical, empirical, semi-empirical, and experimental (other works) of the Coster Kroning transition probability f_{23} from $_{28}$Ni to $_{96}$Cm.

Z, element	This work		Others Work							
			Theo.		Empirical/semi-empirical					
	Emp	MCDFGME	Chen and Crasemann [2]	Chen and Crasemann [37]	Öz et al. [10]	Puri [8]	Campbell [34]	McGuire [23]	Krause [6]	Exp [a]Öz et al. [10] [d]Gupta et al. [38]
$_{28}$Ni	-	0.00685	-	0.0997	-		-	-	0.028	-
$_{29}$Cu	-	0.00455	-	0.1090	-		-	-	0.028	-
$_{30}$Zn	-	0.00972	-	-	-	0.028	-	-	0.026	-
$_{31}$Ga	-	-	-	-	-	0.026	-	-	0.032	-
$_{32}$Ge	-	0.0120	-	0.0249	-	0.025	-	-	0.05	-
$_{33}$As	-	0.0179	-	0.0413	-	0.024	-	-	0.063	-
$_{34}$Se	-	0.0165	-	0.0595	-	0.024	-	-	0.076	-
$_{35}$Br	-	-	-	0.0764	-	0.023	-	-	0.088	-
$_{36}$Kr		0.0067	0.095	0.0922		0.095	0.073	0.0897	0.100	-
$_{37}$Rb	-	-	-	0.107		0.097	0.08	-	0.109	-
$_{38}$Sr	-	-	-	-	-	0.099	0.087	0.115	0.117	-
$_{39}$Y	-	-	-	-	-	0.101	0.094	-	0.126	-
$_{40}$Zr	0.175	-	0.126	0.123	-	0.126	0.100	0.118	0.132	-
$_{41}$Nb	0.174	-	-	-	-	0.129	0.106	-	0.137	-
$_{42}$Mo	0.174	-	-	0.126	-	0.132	0.112	0.124	0.141	-
$_{43}$Tc	0.173	-	-	-	-	0.136	0.118	-	0.144	-
$_{44}$Ru	0.173	-	-	-	-	0.140	0.124	0.136	0.148	-
$_{45}$Rh	0.172	-	0.152	-	-	0.153	0.13	-	0.150	-
$_{46}$Pd	0.171	-	-	-	-	0.154	0.138	-	0.151	-
$_{47}$Ag	0.171	-	0.155	0.130	-	0.156	0.141	0.152	0.153	-
$_{48}$Cd	0.170	0.0960	-	-	-	0.159	0.143	-	0.155	-
$_{49}$In	0.169	-	-	-	-	0.161	0.146	-	0.157	-
$_{50}$Sn	0.168	0.1011	0.166	0.136	-	0.167	0.148	0.162	0.157	-
$_{51}$Sb	0.167	-	-	0.138	-	0.169	0.151	-	0.156	-
$_{52}$Te	0.166	0.1129	0.171	-	-	0.172	0.153	-	0.155	-
$_{53}$I	0.166	-	-	-	-	0.173	0.156	-	0.154	-
$_{54}$Xe	0.165	-	0.174	-	-	0.175	0.159	0.173	0.154	-
$_{55}$Cs	0.164	-	-	-	-	0.177	0.159	-	0.154	-
$_{56}$Ba	0.163	-	0.177	0.151	-	0.178	0.159	-	0.153	-
$_{57}$La	0.162	-	-	-	-	0.176	0.159	-	0.153	-
$_{58}$Ce	0.161	-	-	-	-	0.174	0.158	-	0.153	-
$_{59}$Pr	0.160	-	-	-	0.154	0.172	0.158	-	0.153	
$_{60}$Nd	0158	-	0.170	0.142	0.153	0.171	0.158	0.141	0.152	0.155[a]
$_{61}$Pm	0.157		-	-	0.153	0.168	0.156	-	0.151	-
$_{62}$Sm	0.156	-	-	-	0.152	0.166	0.154	-	0.150	-
$_{63}$Eu	0.155	-	0.162	-	0.150	0.163	0.152	-	0.149	-
$_{64}$Gd	0.154	-	-	-	0.149	0.160	0.150	-	0.147	0.147[a]
$_{65}$Tb	0.152	-	-	0.131	0.148	0.158	0.148	-	0.145	0.150[a]
$_{66}$Dy	0.151	-	-	-	0.146	0.155	0.146	-	0.143	0.145[a]
$_{67}$Ho	0.150	-	0.152	-	0.145	0.153	0.144	0.138	0.142	0.142[a]
$_{68}$Er	0.148	-	-	-	0.143	0.150	0.143	-	0.140	0.141[a]

$_{69}$Tm	0.147	-	-	-	0.142	0.147	0.141	-	0.139	-
$_{70}$Yb	0.146	-	0.143	-	0.140	0.145	0.140	-	0.138	-
$_{71}$Lu	0.144	-	-	-	0.138	0.143	0.138	-	0.136	-
$_{72}$Hf	0.143	-	-	-	0.136	0.141	0.136	-	0.135	0.139[a]
$_{73}$Ta	0.141	-	-	-	0.135	0.139	0.134	-	0.134	-
$_{74}$W	0.140	-	0.139	0.117	0.133	0.140	0.132	0.123	0.133	0.137[a]
$_{75}$Re	0.138	-	-	-	0.131	0.138	0.131	-	0.130	-
$_{76}$Os	0.136	-	-	-	0.129	0.136	0.130	-	0.128	-
$_{77}$Ir	0.135	-	-	-	0.127	0.134	0.128	-	0.126	-
$_{78}$Pt	0.133	-	-	-	0.126	0.132	0.126	-	0.124	0.133[d]
$_{79}$Au	0.131	-	-	-	0.124	0.129	0.125	0.132	0.122	0.125[a]
$_{80}$Hg	0.130	0.1164	0.127	0.108	0.122	0.128	0.123	-	0.120	-
$_{81}$Tl	0.128	-	-	-	0.120	0.126	0.121	-	0.118	0.118[a]
$_{82}$Pb	0.126	-	-	-	0.119	0.123	0.119	-	0.116	0.136[d]
$_{83}$Bi	0.124	0.1109	-	-	0.117	0.121	0.117	0.101	0.113	0.115[a]
$_{84}$Po	0.123	-	-	-	0.116	0.119	0.115	-	0.111	-
$_{85}$At	0.121	-	-	0.100	0.114	0.117	0.113	-	0.111	-
$_{86}$Rn	0.119	0.1064	-	-	0.113	0.114	0.111	-	0.110	-
$_{87}$Fr	0.117	-	-	-	0.112	0.112	0.109	-	0.109	-
$_{88}$Ra	0.115	-	0.110	-	0.111	0.111	0.107	-	0.108	-
$_{89}$Ac	0.113	-	-	-	0.110	0.108	0.105	-	0.108	-
$_{90}$Th	0.111	-	0.106	-	0.109	0.106	0.103	0.102	0.108	0.110[a]
$_{91}$Pa	0.146	-	0.138	-	0.108	0.140	0.141	-	0.139	-
$_{92}$U	0.222	-	0.138	-	0.108	0.139	0.140	-	0.167	0.158[d]
$_{93}$Np	0.265	-	-	0.209	-	0.135	0.136	-	0.192	-
$_{94}$Pu	0.276	-	0.225	-	-	0.228	0.230	-	0.198	-
$_{95}$Am	0.254	-	-	-	-	0.220	0.222	-	0.203	-
$_{96}$Cm	0.200	-	-	-	-	0.212	0.214	-	0.200	-

Table 4: Empirical (this work), theoretical calculations, using the multiconfiguration Dirac-Fock method (MCDFGME), theoretical, empirical, semi-empirical, and experimental (other works) of the Coster Kroning transition probability f_{13} from $_{28}$Ni to $_{98}$Cf.

Z, element	This work		Other works							
			Theo.		Empirical/semi-empirical					Exp
	Emp	MCDFGME	Chen and Crasemann [2]	Crasemann et al [7]	Campbell [35]	Puri [8]	Campbell [34]	McGuire [23]	Krause [6]	[g]Kaur et al. [36] [e]Öz et al. [10]
$_{28}$Ni	-	0.640	-		-	0.334	-	0.622	0.55	-
$_{29}$Cu	-	0.672	-		-	0.334	-	-	0.54	-
$_{30}$Zn	-	0.664	-		-	0.335	-	0.624	0.54	-
$_{31}$Ga	-	-	-		-	0.338	-	-	0.53	-
$_{32}$Ge	-	0.622	-		-	0.354	-	0.671	0.53	-
$_{33}$As	-	0.659	-	0.547	-	0.354	-	-	0.53	-
$_{34}$Se	-	0.650	-		-	0.354	-	0.616	0.52	-
$_{35}$Br	-	-	-		-	0.353	-	-	0.52	-
$_{36}$Kr	-	0.613	-	0.585	-	0.352	-	0.686	0.52	-
$_{37}$Rb	-	-	-		-	0.351	-	-	0.52	-
$_{38}$Sr	-	-	-		-	0.352	-	0.646	0.52	-
$_{39}$Y	0.495	-	0.747		-	0.746	0.57	-	0.52	-
$_{40}$Zr	0.520	-	-	0.522	-	0.747	0.57	0.648	0.52	-
$_{41}$Nb	0.542	-	-		-	0.773	0.57	-	0.61	-
$_{42}$Mo	0.561	-	-	0.692	-	0.771	0.57	0.689	0.61	-
$_{43}$Tc	0.578	-	-		-	0.768	0.57	-	0.61	-
$_{44}$Ru	0.592	-	-		-	0.766	0.57	0.779	0.61	-
$_{45}$Rh	0.604	-	0.759		-	0.759	0.57	-	0.60	-
$_{46}$Pd	0.613	-	-		-	0.750	0.57	-	0.60	-
$_{47}$Ag	0.619	-	0.740	0.695	-	0.740	0.57	0.786	0.59	-
$_{48}$Cd	0.622	0.421	-		-	0.735	0.45	-	0.59	-
$_{49}$In	0.623	-	-		-	0.728	0.45	-	0.59	-
$_{50}$Sn	0.338	0.2997	0.322	0.693	-	0.323	0.30	0.784	0.27	-
$_{51}$Sb	0.330	-	-	0.316	-	0.325	0.25	-	0.28	-
$_{52}$Te	0.322	0.2827	0.326		-	0.328	0.25	-	0.28	-
$_{53}$I	0.315	-	-		-	0.328	0.25	-	0.28	-
$_{54}$Xe	0.309	-	0.328		-	0.329	0.25	0.274	0.28	-
$_{55}$Cs	0.303	-	-		-	0.330	0.25	-	0.28	-
$_{56}$Ba	0.298	-	0.329	0.336	-	0.331	0.25	-	0.28	-
$_{57}$La	0.294	-	-		-	0.328	0.25	-	0.29	-
$_{58}$Ce	0.291	-	-		-	0.328	0.25	-	0.29	-
$_{59}$Pr	0.288	-	-		-	0.321	0.25	-	0.29	-
$_{60}$Nd	0.286	-	0.331	0.332	-	0.332	0.25	0.303	0.30	0.306[e]
$_{61}$Pm	0.285	-	-	-	-	0.331	0.25	-	0.30	-
$_{62}$Sm	0.284	-	-	-	-	0.331	0.25	-	0.30	-
$_{63}$Eu	0.285	-	0.333	-		0.334	0.25	-	0.30	-
$_{64}$Gd	0.286	-	-	-	0.279	0.334	0.25	-	0.30	0.310[e], 0.311[g]
$_{65}$Tb	0.287	-	-	-	0.285	0.334	0.25	-	0.30	0.299[e]
$_{66}$Dy	0.290	-	-	-	0.290	0.335	0.25	-	0.30	0.302[e]
$_{67}$Ho	0.293	-	0.337	0.317	0.296	0.338	0.25	0.309	0.30	0.306[g], 0.314[e]
$_{68}$Er	0.296	-	-	-	0.301	0.354	0.28	-	0.30	0.306[g], 0.309[e]
$_{69}$Tm	0.301	-	-	-	0.306	0.354	0.32	-	0.29	-
$_{70}$Yb	0.306	-	0.352	0.316	0.312	0.354	0.32	-	0.29	-

$_{71}$Lu	0.312	-	-	-	0.317	0.353	0.32	-	0.28	0.316[g]
$_{72}$Hf	0.319	-	-	-	0.322	0.352	0.32	-	0.28	0.290[e]
$_{73}$Ta	0.326	-	-	-	0.328	0.351	0.32	-	0.28	0.323[g]
$_{74}$W	0.334	-	0.350	0.324	0.333	0.352	0.32	0.332	0.28	0.328[g], 0.288[e]
$_{75}$Re	0.457	-	-	-	0.482	0.640	0.32	-	0.33	-
$_{76}$Os	0.484	-	-	-	0.482	0.636	0.33	-	0.39	-
$_{77}$Ir	0.509	-	-	-	0.482	0.631	0.45	-	0.45	-
$_{78}$Pt	0.532	-	-	-	0.545	0.716	0.56	-	0.50	0.563[g]
$_{79}$Au	0.554	-	-	-	0.615	0.711	0.58	0.644	0.53	0.561[g], 0.542[e]
$_{80}$Hg	0.573	0.6317	0.705	-	0.615	0.707	0.60	-	0.56	0.578[g]
$_{81}$Tl	0.591	-	-	-	0.615	0.713	0.60	-	0.57	0.582[e]
$_{82}$Pb	0.606	-	-	-	0.620	0.708	0.61	-	0.58	0.606[g]
$_{83}$Bi	0.620	0.6761	0.700	-	0.620	0.703	0.62	0.656	0.58	0.579[e], 0.603[g]
$_{84}$Po	0.632	-	-	-	0.620	0.697	0.62	-	0.58	-
$_{85}$At	0.642	-	-	-	0.620	0.691	0.63	-	0.59	-
$_{86}$Rn	0.650	0.6761	-	-	0.620	0.685	0.63	-	0.58	-
$_{87}$Fr	0.656	-	-	-	0.620	0.679	0.64	-	0.58	-
$_{88}$Ra	0.660	-	-	-	0.620	0.672	0.65	-	0.58	-
$_{89}$Ac	0.663	-	-	-	0.620	0.666	0.66	-	0.58	-
$_{90}$Th	0.663	-	0.656	-	0.620	0.659	0.66	0.575	0.57	0.577[e]
$_{91}$Pa	0.662	-	-	-	0.620	0.655	0.67	-	0.58	-
$_{92}$U	0.659	-	0.656	-	0.620	0.660	0.67	-	0.57	-
$_{93}$Np	0.654	-	-	-	-	0.656	0.67	-	0.57	-
$_{94}$Pu	0.647	-	-	-	-	0.648	0.68	-	0.56	-
$_{95}$Am	0.638	-	-	-	-	0.639	0.68	-	0.55	-
$_{96}$Cm	0.627	-	0.620	-	-	0.631	0.68	-	0.55	-
$_{97}$Bk	0.615	-	-	-	-	-	-	-	0.54	-
$_{98}$Cf	0.600	-	0.612	-	-	-	-	-	0.54	-

Table 5: Empirical (this work), theoretical calculations, using the multiconfiguration Dirac-Fock method (MCDFGME), theoretical, empirical, semi-empirical, and experimental (other works) of the Coster Kroning transition probability F_{123} from $_{28}$Ni to $_{96}$Cm.

Z, element	This work		Other works					
			Theo.	Empirical/semi-empirical				Exp
	Emp	MCDFGME	Chen and Crasemann [2]	Puri [8]	Campbell [34]	McGuire [23]	Krause [6]	[a]Kaur et al. [36] [b]Öz et al. [10]
$_{28}$Ni	-	0.642	-	-	-	-	0.558	-
$_{29}$Cu	-	0.673	-	-	-	-	0.548	-
$_{30}$Zn	-	0.667	-	0.674	-	-	0.548	-
$_{31}$Ga	-	-	-	0.731	-	-	0.539	-
$_{32}$Ge	-	0.625	-	0.732	-	-	0.544	-
$_{33}$As	-	0.663	-	0.733	-	-	0.548	-
$_{34}$Se	-	0.654	-	0.734	-	-	0.541	-
$_{35}$Br	-	-	-	0.729	-	-	0.545	-
$_{36}$Kr	-	0.615	-	0.723	-	0.700	0.547	-
$_{37}$Rb	-	-	-	0.733	-	-	0.549	-
$_{38}$Sr	-	-	-	0.748	-	0.670	0.552	-
$_{39}$Y	-	-	-	0.756	-	-	0.553	-
$_{40}$Zr	0.563	-	0.758	0.758	-	0.676	0.554	-
$_{41}$Nb	0.585	-	-	0.780	-	-	0.534	-
$_{42}$Mo	0.603	-	-	0.778	-	0.710	0.624	-
$_{43}$Tc	0.618	-	-	0.776	-	-	0.624	-
$_{44}$Ru	0.628	-	-	0.774	-	0.787	0.625	-
$_{45}$Rh	0.635	-	0.768	0.768	-	-	0.625	-
$_{46}$Pd	0.638	-	-	0.760	-	-	0.615	-
$_{47}$Ag	0.633	-	0.751	0.751	-	0.794	0.615	-
$_{48}$Cd	0.525	0.434	-	0.746	-	-	0.606	-
$_{49}$In	0.613	-	-	0.740	-	-	0.606	-
$_{50}$Sn	0.353	0.317	0.353	0.354	-	0.792	0.617	-
$_{51}$Sb	0.347	-	-	0.357	-	-	0.297	-
$_{52}$Te	0.342	0.304	0.359	0.361	-	-	0.308	-
$_{53}$I	0.337	-	-	0.362	-	-	0.308	-
$_{54}$Xe	0.333	-	0.362	0.363	-	0.305	0.309	-
$_{55}$Cs	0.329	-	-	0.365	-	-	0.309	-
$_{56}$Ba	0.326	-	0.364	0.367	-	-	0.309	-
$_{57}$La	0.323	-	-	0.363	-	-	0.309	-
$_{58}$Ce	0.321	-	-	0.363	-	-	0.319	-
$_{59}$Pr	0.319	-	-	0.356	-	-	0.319	-
$_{60}$Nd	0.317	-	0.367	0.366	0.280	0.332	0.319	0.335[b]
$_{61}$Pm	0.317	-	-	0.366	0.280	-	0.329	-
$_{62}$Sm	0.316	-	-	0.366	0.279	-	0.329	-
$_{63}$Eu	0.316	-	0.368	0.369	0.279	-	0.328	-
$_{64}$Gd	0.317	-	-	0.369	0.279	-	0.328	0.338[b]
$_{65}$Tb	0.318	-	-	0.368	0.278	-	0.328	0.328[b]
$_{66}$Dy	0.320	-	-	0.369	0.278	-	0.327	0.330[b], 0.340[a]
$_{67}$Ho	0.322	-	0.370	0.372	0.277	0.337	0.327	0.341[b], 0.336[a]
$_{68}$Er	0.325	-	-	0.381	0.298	-	0.327	0.325[a]
$_{69}$Tm	0.328	-	-	0.381	0.338	-	0.326	
$_{70}$Yb	0.331	-	0.369	0.381	0.338	-	0.316	

$_{71}$Lu	0.335	-	-	0.379	0.337	-	0.316	0.335[a]
$_{72}$Hf	0.340	-	-	0.378	0.337	-	0.304	0.315[b]
$_{73}$Ta	0.345	-	-	0.377	0.337	-	0.304	0.340[a]
$_{74}$W	0.351	-	0.376	0.378	0.337	0.356	0.303	0.313[b], 0.345[a]
$_{75}$Re	0.411	-	-	0.652	0.329	-	0.301	-
$_{76}$Os	0.444	-	-	0.648	0.339	-	0.350	-
$_{77}$Ir	0.475	-	-	0.643	0.459	-	0.409	-
$_{78}$Pt	0.503	-	-	0.725	0.569	-	0.467	0.570[a]
$_{79}$Au	0.528	-	-	0.720	0.589	0.655	0.517	0.561[b], 0.567[a]
$_{80}$Hg	0.549	0.640	0.714	0.716	0.609	-	0.546	0.584[a]
$_{81}$Tl	0.568	-		0.720	0.608	-	0.575	0.599[b]
$_{82}$Pb	0.584	-		0.715	0.618	-	0.584	0.612[a]
$_{83}$Bi	0.597	0.682	0.700	0.710	0.627	0.663	0.592	0.591[b], 0.608[a]
$_{84}$Po	0.607	-	-	0.704	0.627	-	0.592	-
$_{85}$At	0.614	-	-	0.698	0.637	-	0.591	-
$_{86}$Rn	0.618	0.681	-	0.691	0.637	-	0.601	-
$_{87}$Fr	0.619	-	-	0.685	0.647	-	0.591	-
$_{88}$Ra	0.617	-	-	0.678	0.657	-	0.590	-
$_{89}$Ac	0.613	-	-	0.672	0.667	-	0.590	-
$_{90}$Th	0.605	-	0.662	0.665	0.666	0.582	0.590	0.586[b]
$_{91}$Pa	0.594	-		0.662	0.677	-	0.581	-
$_{92}$U	0.580	-	0.663	0.667	0.675	-	0.593	-
$_{93}$Np	0.564	-		0.662	0.674	-	0.583	-
$_{94}$Pu	0.544	-		0.658	0.687	-	0.580	-
$_{95}$Am	0.522	-		0.649	0.687	-	0.570	-
$_{96}$Cm	0.496	-	0.620	0.641	0.686	-	0.558	-

Table 6: Empirical (this work), theoretical calculations, using the multiconfiguration Dirac-Fock method (MCDFGME), theoretical, empirical, semi-empirical, and experimental (other works) of the Coster-Kroning transition probability F_1 from $_{28}$Ni to $_{96}$Cm.

Z, element	This work		Other works						
			Theo.		Empirical/semi-empirical				
	Emp	MCDFGME	Chen and Crasemann [2]	Crasemann [7]	Puri [8]	Campbell [34]	Mcguire [23]	Krause [6]	Exp [a]Kaur et al. [36] [b]Öz et al. [10]
$_{28}$Ni	-	0.923	0.947	-		-	0.947	0.847	-
$_{29}$Cu	-	0.929	-	-		-	-	0.839	-
$_{30}$Zn	-	0.920	0.946	-	0.95	-	0.946	0.831	-
$_{31}$Ga	-	-	-	-	0.931	-	-	0.822	-
$_{32}$Ge	-	0.892	0.938	-	0.926	-	0.938	0.815	-
$_{33}$As	-	0.877	-	0.829	0.922	-	-	0.809	-
$_{34}$Se	-	0.869	0.918	-	0.918	-	0.918	0.804	-
$_{35}$Br	-	-	-	-	0.914	-	-	0.800	-
$_{36}$Kr	-	0.857	0.915	0.81	0.902	-	0.915	0.797	-
$_{37}$Rb	-	-	-	-	0.858	-	-	0.794	-
$_{38}$Sr	-	-	0.894		0.850	-	0.894	0.790	-
$_{39}$Y	-	-	-	-	0.842	-	-	0.785	-
$_{40}$Zr	0.696	-	0.835	0.793	0.835	-	0.884	0.779	-
$_{41}$Nb	0.713	-	-	-	0.828	-	-	0.713	-
$_{42}$Mo	0.726	-	-	0.739	0.827	-	0.855	0.712	-
$_{43}$Tc	0.733	-	-	-	0.825	-	-	0.711	-
$_{44}$Ru	0.736	-	-	-	0.823	-	0.836	0.709	-
$_{45}$Rh	0.732	-	0.821	-	0.821	-	-	0.705	-
$_{46}$Pd	0.724	-	-	-	0.815	-	-	0.700	-
$_{47}$Ag	0.710	-	0.808	0.758	0.808	-	0.838	0.694	-
$_{48}$Cd	0.691	0.557	-		0.806	-	-	0.688	-
$_{49}$In	0.667	-	-		0.802	-	-	0.681	-
$_{50}$Sn	0.557	0.468	0.510	0.765	0.511	-	0.836	0.439	-
$_{51}$Sb	0.544	-	-	0.480	0.515	-	-	0.448	-
$_{52}$Te	0.532	0.467	0.518	-	0.521	-	-	0.455	-
$_{53}$I	0.521	-	-	-	0.523	-	-	0.461	-
$_{54}$Xe	0.511	-	0.524	-	0.526	-	0.453	0.466	-
$_{55}$Cs	0.502	-	-	-	0.529	-	-	0.470	-
$_{56}$Ba	0.494	-	0.529	0.504	0.532	-	-	0.474	-
$_{57}$La	0.486	-	-	-	0.529	-	-	0.478	-
$_{58}$Ce	0.480	-	-	-	0.529	-	-	0.482	-
$_{59}$Pr	0.474	-	-	-	0.522	-	-	0.485	-
$_{60}$Nd	0.470	-	0.54	0.497	0.533	0.440	0.510	0.488	0.494[b]
$_{61}$Pm	0.466	-	-	-	0.542	0.440	-	0.490	-
$_{62}$Sm	0.463	-	-	-	0.543	0.440	-	0.492	-
$_{63}$Eu	0.461	-	0.547	-	0.549	0.440	-	0.493	-
$_{64}$Gd	0.460	-	-	-	0.550	0.440	-	0.493	0.5[b]
$_{65}$Tb	0.460	-	-	-	0.550	0.440	-	0.493	0.49[b]
$_{66}$Dy	0.460	-	-	-	0.552	0.440	-	0.492	0.518[a], 0.497[b]
$_{67}$Ho	0.462	-	0.555	0.495	0.557	0.440	0.511	0.490	0.522[a], 0.501[b]
$_{68}$Er	0.464	-	-	-	0.536	0.405	-	0.487	0.448[a]

$_{69}$Tm	0.468	-	-	-	0.537	0.445	-	0.483	-
$_{70}$Yb	0.472	-	0.468	0.496	0.538	0.445	-	0.478	-
$_{71}$Lu	0.477	-	-	-	0.538	0.445	-	0.472	0.455[a]
$_{72}$Hf	0.483	-	-	-	0.538	0.445	-	0.465	0.472[b]
$_{73}$Ta	0.490	-	-	-	0.537	0.445	-	0.457	0.454[a]
$_{74}$W	0.498	-	0.535	0.484	0.538	0.445	0.527	0.447	0.457[a], 0.471[b]
$_{75}$Re	0.588	-	-	-	0.727	0.390	-	0.485	-
$_{76}$Os	0.612	-	-	-	0.724	0.400	-	0.552	-
$_{77}$Ir	0.633	-	-	-	0.719	0.520	-	0.603	-
$_{78}$Pt	0.651	-	-	-	0.783	0.630	-	0.640	0.616[a]
$_{79}$Au	0.668	-	-	-	0.779	0.650	0.727	0.672	0.611[a], 0.694[b]
$_{80}$Hg	0.683	0.7014	0.774	0.719	0.776	0.670	-	0.690	0.629[a]
$_{81}$Tl	0.696	-	-	-	0.767	0.670	-	0.696	0.73[b]
$_{82}$Pb	0.706	-	-	-	0.762	0.674	-	0.696	0.659[a]
$_{83}$Bi	0.715	0.727	0.7549	0.694	0.758	0.684	0.725	0.694	0.655[a], 0.68[b]
$_{84}$Po	0.721	-	-	-	0.752	0.684	-	0.689	-
$_{85}$At	0.725	-	-	-	0.747	0.694	-	0.685	-
$_{86}$Rn	0.727	0.727	-	-	0.741	0.694	-	0.682	-
$_{87}$Fr	0.727	-	-	-	0.735	0.704	-	0.677	-
$_{88}$Ra	0.725	-	-	-	0.728	0.714	-	0.672	-
$_{89}$Ac	0.721	-	-	-	0.723	0.724	-	0.664	-
$_{90}$Th	0.715	-	0.7135	-	0.717	0.720	0.644	0.660	0.657[b]
$_{91}$Pa	0.707	-		-	0.708	0.720	-	0.664	-
$_{92}$U	0.696	-	0.707	-	0.711	0.705	-	0.652	-
$_{93}$Np	0.684	-	-	-	0.702	0.700	-	0.642	-
$_{94}$Pu	0.669	-	-	-	0.694	0.710	-	0.605	-
$_{95}$Am	0.652	-	-	-	0.686	0.710	-	0.595	-
$_{96}$Cm	0.633	-	0.667	-	0.678	0.710	-	0.587	-